A New Clustering-Based Framework to the Stem Estimation and Growth Fitting of Street Trees From Mobile Laser Scanning Data

Sheng Xu ⬤, Xinyu Sun, Jiayan Yun, and Hao Wang

Abstract—**Estimating individual tree structures from 3-D space may improve the biomass statistics of the urban forest and provide tree-level information for ecological studies. The existing delineation algorithms developed for 3-D point clouds have difficulty in the tree mapping from nonvertical stems or overlapping crowns, and may fail to detect incomplete or occluded branches. Besides, those methods either focus on the individual tree segmentation or crown delineation from the forest, which inadequately estimates the growth fitting of urban street trees. The goal of this article is to present a framework for estimating the growth fitting of street trees' diameter at breast height and under branch height. Tree stems are identified from the achieved street trees' nonphotosynthetic components, including main stems and branches, over different urban trees from mobile laser scanning point clouds. To extract nonphotosynthetic components, a clustering method is proposed to group points from the same stem or branch. The proposed work was validated in both wearable laser scanning data and vehicle laser scanning data, and the experimental scenes contain a range of roadside trees in different structures. In the identification of tree stems, the achieved correctness and completeness are 94.5% and 92.5%, respectively. In the growth fitting, this article calculates a Gaussian model, with the *R*-square up to 0.81, to describe the growth fitting of *Platanus acerifolia*. Results show that the proposed approach succeeds in offering applicability over varying street tree types and the improvement for overlapping individual tree information extraction.**

Index Terms—**Clustering, identification, measurement factor, mobile laser scanning, tree structure.**

I. Introduction

FOR a variety of applications, from growth competition [1], to tree 3-D reconstruction and classification [2]–[4], to biomass estimation [5], [6], and other urban ecological reasons, it is necessary to develop an approach for estimating stem structures from 3-D space to quantify tree presence and distribution.

Sheng Xu is with the College of Information Science and Technology and the College of Landscape Architecture, Nanjing Forestry University, Nanjing 210037, China (e-mail: xusheng@njfu.edu.cn).

Xinyu Sun is with the College of Forestry, Nanjing Forestry University, Nanjing 210037, China (e-mail: 365936972@qq.com).

Jiayan Yun and Hao Wang are with the College of Landscape Architecture, Nanjing Forestry University, Nanjing 210037, China (e-mail: yunjiayan@snu.ac.kr; wh9816@126.com).

The classical estimation of tree structure usually depends on 2-D imagery information [7], [8]. To quantify urban tree cover at the street level, the relationship between neighboring images along with street segments is modeled in urban environments, and then, the amount of perceived tree cover is estimated. The problem is that the tree stem and branch information are difficult to collect. Nowadays, Light Detection And Ranging (LiDAR) point clouds become mature in terms of the density, efficiency, and cost-effectiveness of the data collection, which describes 3-D information of objects accurately and becomes popular in organizing point clouds back into trees.

According to the scanner platforms, LiDAR technique can be divided into terrestrial laser system (TLS), airborne laser system (ALS), and mobile laser system (MLS) [9]. ALS is a method based on LiDAR range measurements from an aircraft and sensors to obtain the position of which is (x, y, z). The ALS gives the georeferenced point cloud, from which it is possible to calculate digital terrain models and digital surface models corresponding to treetops for forest measurements. TLS is based on LiDAR range measurements from a scanning system mounted on a tripod, which is usually chosen for the individual tree modeling [10]. MLS is relatively new, which is required to be mounted on a piece of moving equipment, e.g., vehicles (vehicle laser scanning, VLS) or simply human beings (wearable laser scanning, WLS). Those LiDAR techniques have different benefits and limitations in urban tree analysis. TLS collects plentiful of the tree stem and branch information, but are highly affected by understorey shrubs and the user has to set a plot for street trees in every 8–10 m. ALS deals with a city-scale of the point cloud collection efficiently, but has visibility problems in the collection of tree stems caused by canopy closure. To balance the collection efficiency and the tree side information adequacy, this article chooses MLS for the data collection, including WLS and VLS. WLS is flexible to obtain the region of interest (ROI) points, e.g., the back of trees and tree base. VLS is feasible to obtain most tree side information at a speed of 30 km/h.

The target of this article is to provide a new framework for estimating the growth fitting of street trees. Contributions are in threefold, which are as follows.

1) Estimating the growth fitting of street trees to provide an example for validating the fitting of the tree structure.
2) Mapping the nonphotosynthetic components of street trees from WLS and VLS data, and show the comparison of mapping results between them.

3) Developing a new clustering method for mobile laser scanning data to group points from the same stem.

II. RELATED WORK

Currently, there have been a lot of schemes provided for the analysis of tree structure and parameters from different forest ecosystems. Several related studies on point cloud processing for estimating tree structures are as follows.

In the segmentation of tree stems, the target is to achieve points from the lowest point of an individual tree to its first branch. Lehtomaki *et al.* [11] proposed a method based on the segmentation and clustering of scanning lines to extract stems from VLS data. Their detection accuracy depends on the prior knowledge of stems, such as tree height, position, and number, which is easily affected by the crown density. Arachchige [12] designed a 3-D operator based on the direction and geometry information of trunks to measure similarity of points. This method does not need the prior knowledge of trees and can be applied to different trunks. However, their region growing process of tree trunks cannot be applied to incomplete stem points. Liang *et al.* [13] proposed a stem extraction method based on a 3-D cylindrical model. Their method is suitable for extracting vertically stand trunks, which means tree stem points are most likely from a vertical planar structure, and is easily affected by point cloud density. Xia *et al.* [14] proposed an extraction method based on multiscale geometric features from TLS data, which does not need any model fitting process. Their stem points are identified with a classification process based on geometric features, such as shape and size. Zhong *et al.* [15] proposed a canopy segmentation method to split the overlapping regions of trees. Their stem detection and the overlapping region segmentation is achieved by a complex parameter setting process.

In the segmentation of individual trees, the target is to achieve an independent trunk, branch, and crown for providing tree attributes, such as position, number of trees, and tree height. Pu *et al.* [16] present a knowledge-based feature recognition method for structure recognition from point clouds. Based on a series collection of characteristics of point cloud segments, such as size, shape, orientation, and topological relationships, the objects on the ground are assigned to more detailed classes, such as traffic signs, trees, building walls, and barriers. Li *et al.* [17] proposed a region growing method from top to bottom to extract targets, which assigns neighborhood points near the top of the tree to the selected tree vertices by setting thresholds. Since nonstems have been removed by a coarse classification process, two components of each individual tree, i.e., a trunk and a crown, can be extracted by their method. However, for low-level points, it is difficult to segment overlapping trees by setting a single threshold. Vega *et al.* [18] proposed a segmentation method by selecting the best neighborhood range at the tree vertex with frequent human interaction. To improve the effectiveness of the tree crown delineation, Hu *et al.* [19] developed a framework to split tree crowns based on a canopy height model, including the determination of dominant crown sizes, the generation of initial tree segments, and the refinement of the nontree segments by splitting and merging operations. Although their method

obtains a large-scale tree crowns effectively, results from ALS data contain little trunk information. Chen *et al.* [20] present a feasible workflow for urban tree inventory from MLS data, including the crown diameter, diameter at breast height (DBH), and tree height. Their algorithm first extracts individual tree clusters and then estimates geometric parameters for tree species classification. The potential issue is that uneven point density in the MLS data may result in problems for their segmentation algorithm based on Euclidean distances between nearest points.

In the segmentation of nonphotosynthetic components of trees, the target includes the main trunk and branches, which is important to study the growth of urban forest. Raumonen *et al.* [21] proposed a tree trunk and branch modeling method from TLS based on the cylinder fitting. By building the cylinder model of trees, the branch structure of the whole tree is approximately obtained from the model. Similarly, Hackenberg *et al.* [22] proposed a method to extract cylindrical fitting points from TLS data. Their model takes high scanning quality data as input, describes the branch structure of the tree, and detects branches with diameter less than 1 cm. The limitation lies in the part with low density, where the cylinder fitting accuracy will inevitably decrease. Since point clouds are unorganized, Wu *et al.* [23] present a voxel-based neighborhood searching method for identifying street trees. The disadvantage is that its voxel-based segmentation method often divides the nonphotosynthetic components of the same tree into several trees in a complex mixed forest, i.e., oversegmentation. Tao *et al.* [24] adopted a density-based spatial clustering of applications with noise (DBSCAN) for trunk segmentation. Their nonphotosynthetic components of trees are distributed point by point according to the distance only. Fan *et al.* [25] present an automatic algorithm to localize and extract urban trees from their formulated supervoxels. Geometry information of the object are calculated within the supervoxel, including pole features and trunk features. Palm trees from MLS data are extracted effectively by setting thresholds based on the shape and distance information. The problem with Tao *et al.* [24] and Fan *et al.* [25] is that they need to accurately locate the position of the trunk, which depends on the density of the points and the shape of the trunk.

In the modeling of 3-D trees, the target is to build tree stems and branches from 3-D space. Livny *et al.* [26] present an approach that reconstructs skeletal structures of trees to capture full geometry information. They develop a series of global optimizations to fit skeletal structures for noisy point data. Although their approach has the ability to reconstruct multiple overlapping trees simultaneously, it fails to reconstruct skeletal structures over large regions of missing data. Zhang *et al.* [27] developed a data-driven technique to model trees from TLS data. They propose a multilayer representation of the tree structure and develop a cylinder algorithm to construct visible branches point cloud data. The limitation is that it is difficult to deal with distorted and wired branches by a single angle adjustment. In order to address the modeling issue of incomplete TLS data, Wang *et al.* [28] proposed a method based on a structure-aware global optimization approach to obtain the approximate tree skeleton. The key to their methods lies in the definition of a distance minimum spanning tree and the stretching directions of
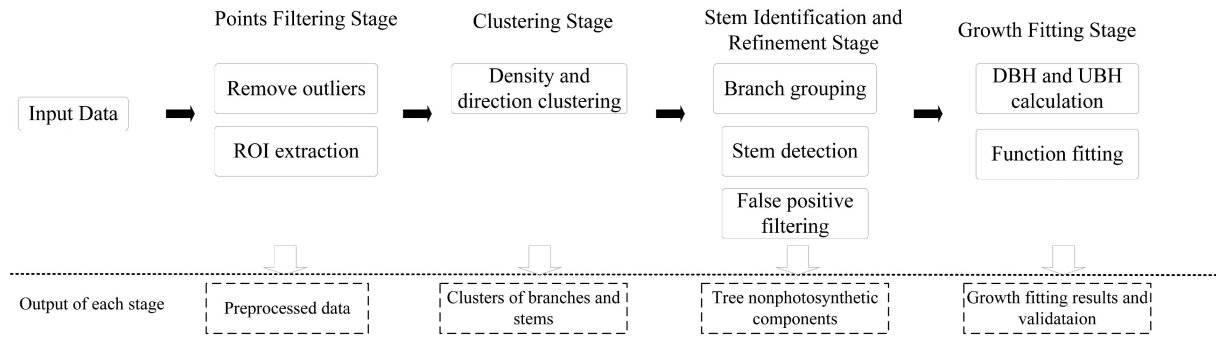
Fig. 1.　Flowchart of the proposed growth fitting approach.

the branches on the tree skeleton. Based on stretching directions, they recover missing data from the incomplete point cloud. The limitation is that users need to build a directed graph to deal with the potential ring structure caused by the overlapping of tree branches. Later, Wang *et al.* [29] used a local structure and direction-aware approach to complete missing structures of trees. They build a local tree structure to describe tree structures and geometrical relationship among branches and use the information of dominant direction and point density to recover the missing data. Although their method is less sensitive to incomplete and noisy data, the performance of tree modeling on large-scale scenes with equally high quality is difficult. Besides, their accuracy also depends on the plant growth parameters and those higher elevation branches are easy to be synthesized with low quality when tree branch directions are various.

Currently, the existing algorithms had difficulty in the distinguishment of nonvertical tree stems and the split of overlapping branches from point clouds. Limitations of the existing algorithms lie in the following.

1) Algorithms have weak robustness, limited application scenarios, and cannot be applied in complex scenarios.
2) Algorithms cannot deal with the problem of data incompleteness and occlusion.
3) Algorithms require the complex parameter adjustment process, such as tree position, number, height, and crown shape.

It is difficult to find optimal parameters, so results are prone to appear undersegmentation or oversegmentation. This limits the application of laser scanning data in urban forest resource management, especially in the statistics of street trees.

Motivated by the fact that the point density and direction between nonphotosynthetic components and tree leaves are quite different, researchers have developed lots of region growing methods to extract trunks. For example, Xu *et al.* [30] proposed a hierarchical clustering method to extract nonphotosynthetic components from urban scenes. To address potential issues in the clustering [31], e.g., the slow convergence rate and easily dropping in local minima, the combination of nonphotosynthetic component points is globally optimized by a Hopfield neural network at a high computation complexity. To reduce the optimization complexity and address disadvantages in the existing clustering methods, e.g., highly depends on the tuning of parameters and the initialization of centers, this article presents a new clustering method to group stem and branch points. After

we obtain the nonphotosynthetic components of street trees, we provide a scheme for the analysis of structural parameters of roadside trees from urban environments, which is promising in the urban forest management.

III. ESTIMATION OF THE GROWTH FITTING

This section aims to present an approach for estimating the structure parameters of the urban forest and providing the growth fitting of street trees' nonphotosynthetic components. The flowchart of this work is shown in Fig. 1. The input urban street scene is collected by MLS containing buildings, urban forests, roads, vehicles, etc. There are four main stages, namely the point filtering, clustering, stem identification and refinement, and growth fitting. Details of those stages will be discussed in the following sections one by one.

A. Points Filtering Stage

This stage is the preprocessing step of the proposed framework, which refines and prunes data to improve the accuracy and efficiency. The first part is the data denoising to remove outliers based on the statistical information of the point Euclidean distance. A point is considered to be an outlier if the average Euclidean distance μ to its k-nearest neighbors is above a user-defined threshold. The setting of the threshold is based on the standard deviation σ of distance. In our work, points fall out of $\mu \pm \sigma$ will be regarded as outliers. The second part is the extraction of the ROIs to reduce the scale of input points. The input scene is fixed as urban streets and the target lies in the region of street trees. Therefore, we prefer to remove ground points and building facades based on the plane fitting before the extraction process. This is solved by the existing method [32], which uses an agglomerative hierarchical clustering to group nodes and fit planes.

In our test, the denoising step can remove 3%–5% points from the input MLS point clouds, which depends on the scanner, traffic condition, and types of street trees. Although there are small planes in the preprocessed data, we can distinguish trees from planes in the stem identification stage easily.

B. Clustering Stage

This section aims to provide a new clustering method to address disadvantages in the existing point cloud clustering and
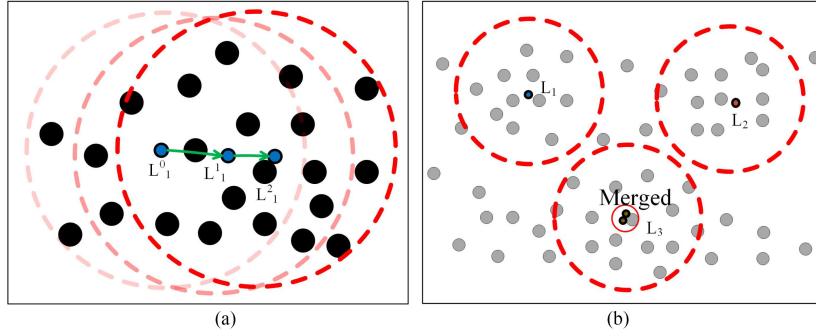
Fig. 2. Iteration of the clustering approach. (a) Update of the center point. (b) Achieved three centers.

region growing process. The key idea is to regard each point as a cluster center at the beginning of the clustering stage, and then update coordinates of cluster centers iteratively based on the local density and direction of points. If two centers are spatially close, these two centers will be merged. Finally the number and coordinates of centers are converged and stable, which means all centers of clusters are found. There is no need to input the number of clusters and the challenge is to update the coordinate of centers. Detail steps of the proposed clustering are shown as follows.

1) Choose an unlabeled point at (x, y, z) from input data and let the coordinate of the current center as $L_i = (x, y, z)$.
2) Calculate the sum of distances between neighbors p_i and the current center as $\mathbf{V}_i = \Sigma H(p_i, L_i, h) \cdot L_i$, where h will indicate the region of neighbor points.
3) Update the coordinate as $L_i = L_i + \mathbf{V}_i$ by moving the current point along the vector $\mathbf{V}_i$.
4) Iterate the aforementioned steps 1)–3), until the achieved $\mathbf{V}_i$ is vanished, i.e., the number and coordinate of centers are converged.
5) Assign points of input to the converged centers based on Euclidean distance information.

In step 2), the function $H(p_i, L_i, h)$ is to weigh the distance of neighbors to the current center. In K-means approach, the weight of each point to its center is the same. However, the contribution of each point should take the density and plane direction of neighbors into consideration. Besides, the kernel function $H(p_i, L_i, h)$ is required to be nonnegative, nonincreasing, and piecewise continuous. Therefore, we formulate the required function as the following Gaussian kernel:

$$H(p_i, L_i, h) = \frac{\cos <p_i, L_i>}{\sqrt{2\pi}h} e^{-\frac{\|p_i - L_i\|^2}{2^-h^2}} \tag{1}$$

where h is the user-defined bandwidth to set the region of neighbors. A large h will set a wide range of neighbors but with a small weight for neighbors. A small h causes a narrow range of neighbors, but with a large weight of points that are spatially close to the center. $\cos <p_i, L_i>$ measures the difference of the normal vector direction at the neighbor point p_i and L_i. The normal vector at a point is approximated as the normal to the surface estimated by its neighbors.

The proposed clustering is an iterative process. The first step is to initialize each point as a center. Then, translate the current center to a denser region. Start from the new center to continue

the iteration until centers are converged, as shown in Fig. 2(a). Finally, spatially close centers will be merged into one unit. Points of the same center are grouped into the same cluster, as shown in Fig. 2(b). Similar to the K-means approach, we are also required to update center points. The difference lies in the fourfold.

1) The number of clusters is automatically decided in the proposed clustering.
2) Our weight for the distance from neighbors to centers is more suitable for point clouds.
3) The proposed clustering can deal with any shapes of clusters, e.g., convex or nonconvex clusters.
4) Compared with DBSCAN method, there is only one constant parameter h to be set in the algorithm, which makes the setting of parameters easier.

C. Stem Identification and Refinement Stage

This stage aims to merge branch and stem points of the nonphotosynthetic components from the same tree. The first part is the branch growing. At the beginning of the growing process, each center is regarded as one branch. Branches that are spatially close and sharing the same direction are grouped into one unit. For a center L_1, the merging branch approach first finds its neighbors, i.e., $L_2, L_3, \ldots, L_k$. Then, the algorithm calculates the Euclidean distance and elevation distance between L_1 and L_n, which is denoted by $D(p_1, p_n)$ and $E(p_1, p_n)$, $n = 2, 3, 4, \ldots, k$, respectively. Then, the algorithm calculates the value of $\frac{E(p_1, p_n)}{D(p_1, p_n)}$ and find the max value at L_j. Merge points that choose L_1 and L_j as their centers into the same branch. Repeat this step, until all centers are traveled.

The second part is the detection of main stems to find the candidate roots of trees based on elevation filtering. If the lowest point of a branch is less than 1 m, this branch will be regarded as a candidate root. We assign the aforementioned grouped branches to their spatially close roots.

The third part is to remove false trees based on the following simple rules.

1) Tree Height: If the height of the extracted nonphotosynthetic component is low, e.g., less than 2 m, this component will be marked as false positive (FP). This rule is to remove polelike objects with a low elevation, e.g., traffic signs or statues.
2) Tree Points: If the number of points from the extracted nonphotosynthetic component is small, e.g., less than 100
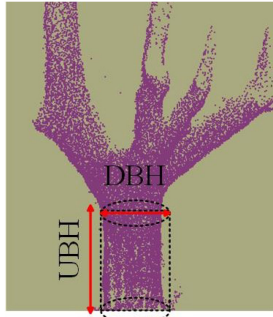
Fig. 3.   Calculation of DBH and UBH based on the extracted nonphotosynthetic components.

points, this component will be marked as FP. This rule is to remove tree ghosts result from registration error and small shrubs.

3) Tree Distribution: The distinguish between trees and other polelike objects is based on the points distribution in the vertical direction. We calculate the vertical kurtosis [15] for the mapped nonphotosynthetic components to remove FP components. If the kurtosis of a nonphotosynthetic component falls in $\mu_k - 1.5\delta_k$ and $\mu_k + 1.5\delta_k$, it will be regarded as a valid component. μ_k and δ_k are the mean and standard deviation of the kurtosis of all extracted nonphotosynthetic components. This rule is to remove polelike objects at a high elevation, e.g., traffic lamps.

D. Growth Fitting Stage

There are two key growing parameters of street trees, i.e., the DBH and under branch height (UBH). The DBH is a standard and the most common parameter of measuring tree dimensions apart from tree height. It can be applied to monitor the growth of trees and compare the dimensions of different trees. Formally, DBH refers to the diameter of a tree trunk measured at breast level, which is a convenient way of measurement. The UBH is used to measure the height to first branch. The calculation of DBH and UBH observed in the study fields is based on the cylinder fitting for each achieved individual tree nonphotosynthetic component, as shown in Fig. 3. In point cloud processing, one can solve the cylinder fitting based on the random sample consensus (RANSAC) method [33] directly. The RANSAC method extracts shapes by randomly drawing minimal sets from the input data and constructing corresponding shape primitives. The radius and height of the fitted cylinder is regarded as DBH and UBH, respectively.

IV. Experiments and Discussion

A. Experimental Scene and Dataset

This section shows the performances of the proposed method on MLS point clouds, including WLS and VLS dataset. Experiments are in twofold. The first is the results of the stem identification from MLS data and the second is the validation

and growth fitting of DBH and UBH. Before the evaluation, we give a brief description of the input scenes and scanner.

The first dataset is collected by us using a WLS system. The WLS device used to perform the study was the ZEB-REVO mobile laser scanner commercialized by GeoSLAM.[1] The batteries and the data storage and processing units are located in a small backpack. The system acquires 3-D information of the input urban scene effectively. The range of the scanner is from 0.6 to 30 m, the scanner weight is 850 g, the scanner point frequency is 43 000 points/s, the relative accuracy is 1–3 cm, and the raw data file size is 100 MB/min. The experimental scene is located in Huangpu Road, Nanjing, China, at the geolocation of (118.81 E, 32.04 N), the length of the road is 643 m, and the collection date in July 30, 2019. The WLS dataset contains 118 individual trees and 151 430 412 points, as shown Fig. 4. Fig. 4(a) demonstrates the top imagery view of the input scene. Fig. 4(b) demonstrates the 3-D point clouds of the input scene. The red trajectory shows how to walk around trees with the scanner to get enough view and, hence, point clouds of sufficient point densities. The registration of the collected WLS point clouds is achieved by the algorithm integrated by GeoSLAM. In order to improve the registration accuracy, we conduct the data collection for every 150 m along the road. Therefore, the input scene is present as four plots. Fig. 4(c) shows the point cloud of an individual street tree from this urban scene. The top one is the point collection of the tree and the bottom is the manually segmented nonphotosynthetic component.

The second dataset is chosen from an open benchmark located in Paris collected by a vehicle laser scanning system in January 2013. The imagery and a point cloud of the test scene are shown in Fig. 5(a) and (b), respectively. The red trace in Fig. 5(a) is the simulated trajectory based on the density from VLS data. The size of the test data is 173 m by 352 m containing 49 512 718 points and 187 individual trees. Detail description of the data collection is shown in [34]. Fig. 5(c) shows the a point cloud of an individual street tree (left-hand side) and its nonphotosynthetic component (right-hand side).

B. Results of the Stem Identification

Our stem identification results of WLS are shown in Fig. 6. Each stem is visualized by a unique color. We achieve 118/118 individual trees from input data. If 80% points of a stem is identified, this stem is regarded as extract correctly. The stem identification results from VLS data are shown in Fig. 7. Different from data collected by WLS, the density of points is less. Besides, the distance between the sensor and trees are various from 3–30 m. Fig. 7 is the results of all stems from the VLS data. We succeed in achieving 154/182 individual trees stems input data. As shown in Fig. 7, from the plot 1–6, we identify 19/21, 19/19, 12/12, 13/13, 10/15, and 10/12 stems. We distinguish trees and polelike objects in plot 1, but miss the incomplete stems. Plots 5 and 6 demonstrate a very complex scene containing different types and height of trees. The achieved stem is very thin. Different types and height of trees are overlapped with each

---

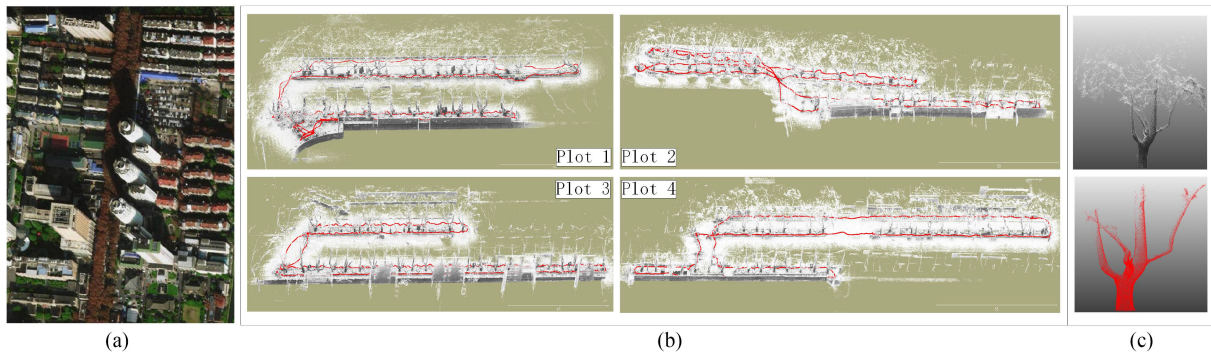[1]Online. [Available]: http://geoslam.com/hardware-products/zeb-revo/

Fig. 4. Description of the input scene collected by the wearable laser system. (a) Imagery of the test scene @Baidu 2020 map data. (b) Point cloud of the test scene for the plots 1–4. The red line is the trajectory. (c) Illustration of an individual street tree (top) and its nonphotosynthetic component obtained by manual (bottom) from WLS data.
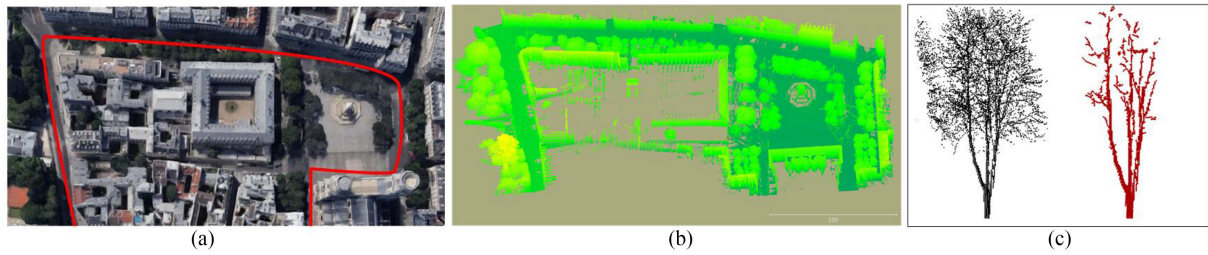

Fig. 5. Description of the input scene collected by the vehicle laser system. (a) Imagery of the test scene @Google 2020 map data (48°51'01.3"N, 2°19'57.9"E). The red line is the manually generated vehicle trajectory based on the point density. (b) Point cloud of the test scene. (c) Illustration of an individual street tree (left-hand side) and its nonphotosynthetic component obtained by manual (right-hand side) from VLS data.
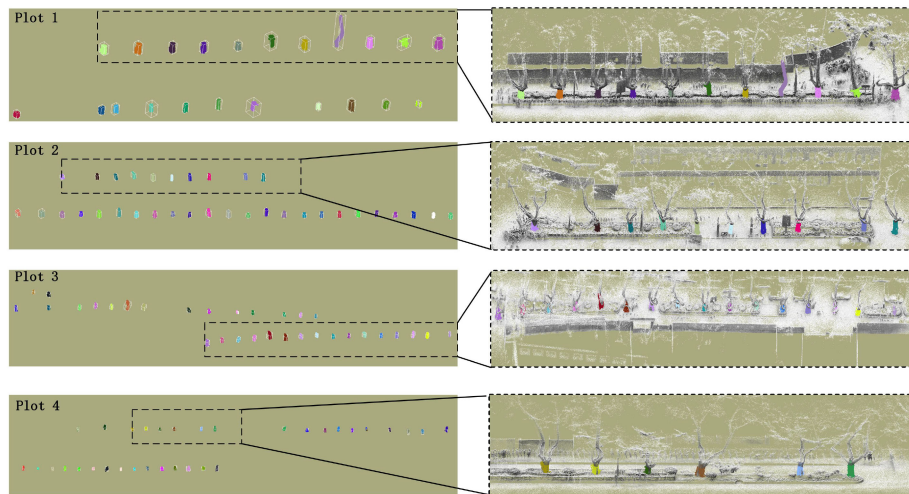

Fig. 6. Achieved stems under the branch. (a)–(d) Results of the plots 1–4 corresponding to Fig. 4.

other, which makes the stem identification extremely difficult. In our results of VLS data, if street trees are close to the vehicle LiDAR sensor (<10 m), trunks and branches of a tree will be completely extracted. However, if trees are far from the sensor (>30 m), extraction results may only contain the main stem and branches of a tree due to the sparsity of tree points. WLS enables users to flexible obtain the side information of a large-scale trees efficiently; therefore, there is little data incompleteness and occlusion in the stem identification from WLS data. However, as shown in the region 5 of Fig. 7, the incomplete and occluded trees appear in VLS data. In this case, if tree trunks contain dominant direction information, the proposed clustering can track the main trunk to group points together, as shown in the region 6 of Fig. 7.

C. Evaluation of Identification Results

In order to evaluate the extraction, the result of a point is divided into true positive (TP), false negative (FN), and FP. TP means that a stem point is extracted correctly from the input scene. FN means that a stem point is wrongly detected as the background point. FP means that a background point is wrongly recognized as a stem point. The ground truth of
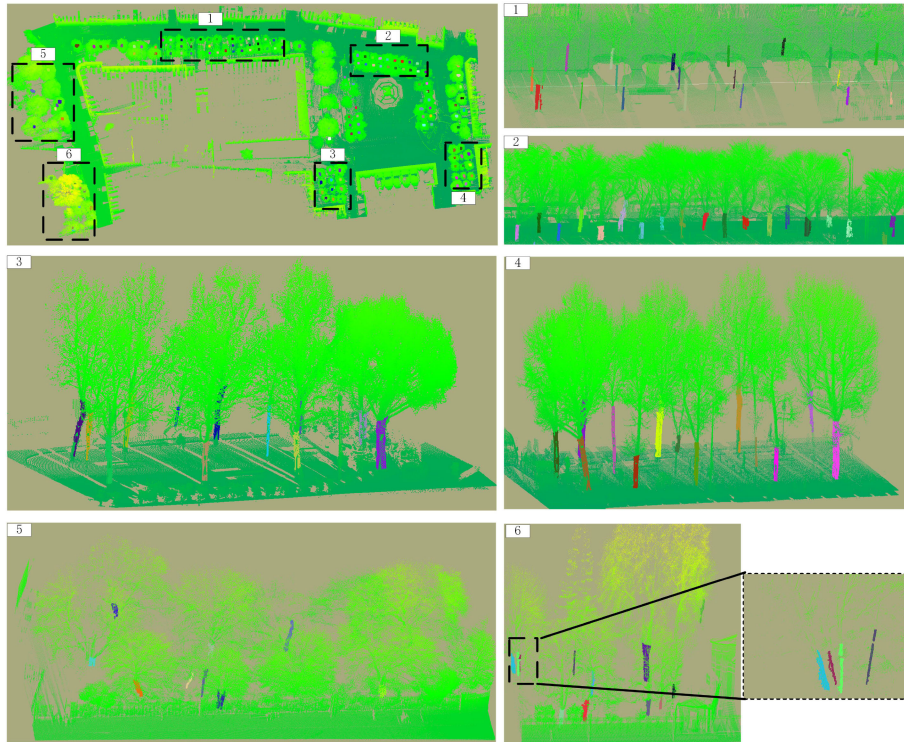
Fig. 7.   Achieved stems under the branch. (1)–(6) Close views of the region 1–6 corresponding to Fig. 5.

nonphotosynthetic components for the reference is obtained manually from the input scene. We segment the stem of each individual tree attentively through the point cloud visualization tool CloudCompare [2] manually. The following aims to compare and discuss the performance of the stem identification and other methods. For the evaluation, we calculate the correctness r, completeness p, and F-score f as

$$r = \frac{\text{TP}}{\text{TP} + \text{FP}}, p = \frac{\text{TP}}{\text{TP} + \text{FN}}, f = \frac{2 \times \text{TP}}{2 \times \text{TP} + \text{FP} + \text{FN}}. \quad (2)$$

The correctness measures the ratio of correctly detected stems in results, and the completeness measures the percentage of correctly extracted stems in the reference. F-score is the harmonic mean of correctness and completeness.

In order to demonstrate the identification accuracy of the proposed method, we show the comparison with the other related methods, including [11]–[17], [19], [20], [23]–[25], [28], and [30]. Since the extraction of roadside trees from MLS adopts the same methods used for extraction roadside light-poles or polelike objects, especially for deciduous trees in winter, we choose two more learning-based polelike object detection methods in the comparison, i.e., Guan *et al.* [35] and Wu *et al.* [36]. Table I lists the description of datasets and test scenes in the aforementioned segmentation methods. The scanner shows the collection system. Density D is calculated by the number of points per square meter close to road surface. The environment shows the region of data collection, including the urban, residential, forest, etc. The ToO means the type of objects, including

multiple street trees (MST), homogeneous street trees (HST), multiple forest trees (MFT), homogeneous forest trees (HFT), and polelike object (PO). The NoO means the number of objects. The DoC means the date of collection. The Target means the segmentation results. Some of methods are tested in different plots as denoted by # 1, 2, 3..., as shown in Table I. Quantitative results of the aforementioned methods are shown in Table II. Our achieved average correctness, completeness, and F-score on two datasets are 94.5%, 92.5%, and 0.94, respectively.

In the comparison, although the accuracy of Arachchige [12], Li *et al.* [17], Wu *et al.* [23], Tao *et al.* [24], and Fan *et al.* [25] seem better than ours, the number and type of trees in their experimental scene are less than ours, as shown in Figs. 6 and 7. Compared with the polelike object extraction, the proposed method is more accurate than Guan *et al.* [35]. Although our accuracy is lower than Wu *et al.* [36], we do not need to build training samples, i.e., 3303 samples in Wu *et al.* [36].

The aforementioned extraction was done on a Windows 10 Home 64-bit, Intel Core i7-4790 3.6-GHz processor with 16 GB of RAM and computations were carried on MATLAB R2019b. Be aware that it is difficult to run the aforementioned methods on our dataset due to the fact that accuracy depends on the parameter setting. We give the detail description of their experimental scenes and provide the evaluation results for users to choose methods based on their applications.

D. Evaluation of the Growth Fitting Results

The ground truth of stems' DBH and UBH from WLS is achieved by using a tape measure in the experimental plot. For

[2]Online. [Available]: http://www.danielgm.net/cc/

TABLE I
DESCRIPTION OF DATASETS IN DIFFERENT METHODS

Methods	Scanner	Dataset D(points/m2)	Environment	Test Scene ToO	NoO	DoC	Target
Lehtomaki *et al.* [11]	MLS	NULL	suburan	NULL	79	NULL	trunk
Pu *et al.* [16]	MLS #1	NULL	urban	MST	33	12/2018	stem & crown
	MLS#2	NULL	urban	MST	84	06/2009	stem & crown
Wu *et al.* [23]	MLS#1	212	residential	HST	72	03/2012	stem & crown
	MLS#2	224	residential	HST	68	12/2012	stem & crown
Hetti *et al.* [12]	MLS	NULL	urban	MST	42	NULL	stem
Liang *et al.* [13]	MLS	NULL	forest	MFT	80	NULL	stem
Xia *et al.* [14]	TLS	1000	forest	HFT	166	11/2013	stem
Tao *et al.* [24]	TLS#1	NULL	garden	MST	14	02,09/2014	stem & crown
	TLS#2	NULL	forest	HFT	51	12/2014	stem & crown
	TLS#3	NULL	forest	HFT	49	01/2015	stem & crown
Li *et al.* [17]	MLS#1	123	urban	MST	66	NULL	stem & crown
	MLS#2	306	urban	MST	29	NULL	stem & crown
Zhong *et al.* [15]	TLS	2821	university	MST	157	01/2015	nonphotosynthetic
	MLS	222	urban	MST	519	06/2011	nonphotosynthetic
Wu *et al.* [25]	MLS	NULL	urban	HST	311	NULL	stem & crown
Xu *et al.* [30]	MLS	700	urban	MST	182	01/2013	nonphotosynthetic
Hu *et al.* [19]	ALS	NULL	forest	MFT	NULL	08/2009	tree crown
Chen *et al.* [20]	MLS	>9000	urban	MST	163	Various	stem & crown
Wang *et al.* [28]	TLS	NULL	urban	MST	22	NULL	stem & crown
Guan *et al.* [35]	MLS	NULL	urban	PO	888	NULL	lightpole & traffic signpost
Wu *et al.* [36]	MLS	NULL	urban	PO	NULL	NULL	lightpole
Proposed	MLS#1	1000	urban	HST	118	07/2019	stem
	MLS#2	700	urban	MST	182	01/2013	stem

TABLE II
COMPARISON RESULTS OF THE AFOREMENTIONED METHODS

Evaluation	Lehtomaki *et al.* [11] MLS	Pu *et al.* [16] MLS#1	MLS#2	Avg.	Wu *et al.* [23] MLS#1	MLS#2	Avg.	Hetti *et al.* [12] MLS	Liang *et al.* [13] MLS	Xia *et al.* [14] TLS
r(%)	86.5	84.6	85.7	85.2	100	100	100	97.5	/	93.0
p(%)	83.5	63.5	29.5	46.5	100	98.5	99.3	92.5	87.5	88.0
f	0.85	0.73	0.44	0.59	1.00	0.99	1.00	0.95	/	0.90

Evaluation	Tao *et al.* [24] TLS#1	TLS#2	TLS#3	Avg.	Li *et al.* [17] MLS#1	MLS#2	Avg.	Zhong *et al.* [15] TLS	MLS	Avg.
r(%)	100	100	92.0	97.3	98.4	97.4	97.9	92.4	94.0	93.2
p(%)	100	100	100	100	98.2	96.8	97.5	95.4	93.7	94.6
f	1.00	1.00	0.96	0.99	0.98	0.97	0.98	0.94	0.94	0.94

Evaluation	Wu *et al.* [25] MLS	Xu *et al.* [30] MLS	Hu *et al.* [19] ALS	Guan [35] MLS	Wu *et al.* [36] MLS	Proposed MLS#1	MLS#2	Avg.
r(%)	89.0	98.9	73.0	88.9	99.4	96.2	92.7	94.5
p(%)	86.2	94.0	88.0	88.9	97.9	94.6	90.4	92.5
f	0.88	0.96	0.80	0.89	0.98	0.95	0.92	0.94

each plot from 1 to 4, we measure the DBH and UBH of trees randomly for several times and use the average DBH and UBH as the ground truth for the fitting. In the analysis of the mapping error, we choose the root-mean-squared error (RMSE) and the coefficient of determination *R*-squares (0–1) as defined in (3) and (4), respectively

$$\text{RMSE} = \sqrt{\frac{1}{n} \sum_{i=1}^{n} \left(G_i' - G_i \right)^2} \qquad (3)$$

$$\text{R-square} = \frac{\sum_{i=1}^{n} \left(G_i' - \overline{G} \right)}{\sum_{i=1}^{n} \left(G_i - \overline{G} \right)} \qquad (4)$$

where G_i' is the estimated results, G_i is the ground truth, and $\overline{G}$ is the mean value of the ground truth. The fitting function between DBH and UBH is a linear function as

$$f(x) = p_1 \cdot x + p_2. \qquad (5)$$

The evaluation figure is shown in Fig. 8, including the fitting function and residuals. In the evaluation of DBH, our RMSE is

9.46 cm and *R*-square is 0.58 (with 95% confidence bounds), the achieved p_1 is 0.70 and p_2 is 18.13. In the evaluation of UBH, the RMSE is 36.75 cm and *R*-square is 0.46 (with 95% confidence bounds), the achieved p_1 is 0.64 and p_2 is 84.62.

As mentioned in Section III-D, the calculation of DBH and UBH is based on the cylinder fitting. In our test, if the inlier points in RANSAC are more than 60% of input nonphotosynthetic components, we can achieve the DBH and UBH accurately. For the DBH and UBH comparison, although our achieved *R*-square might be lower than TLS-based method, for example, compared with Wang *et al.* [28], the number of trees between ours and Wang *et al.* [28] is 118 versus 22. In the method of Chen *et al.* [20], their MLS-based method achieves the *R*-square of 0.60 on 183 trees, which is more accurate than ours in terms of DBH calculation. However, consider the relative standard deviation calculated by the ratio of RMSE and the average DBH, our result is better than theirs, i.e., 0.11 versus 0.14. This is because we balance the dominate direction information and Euclidean distance in the clustering.
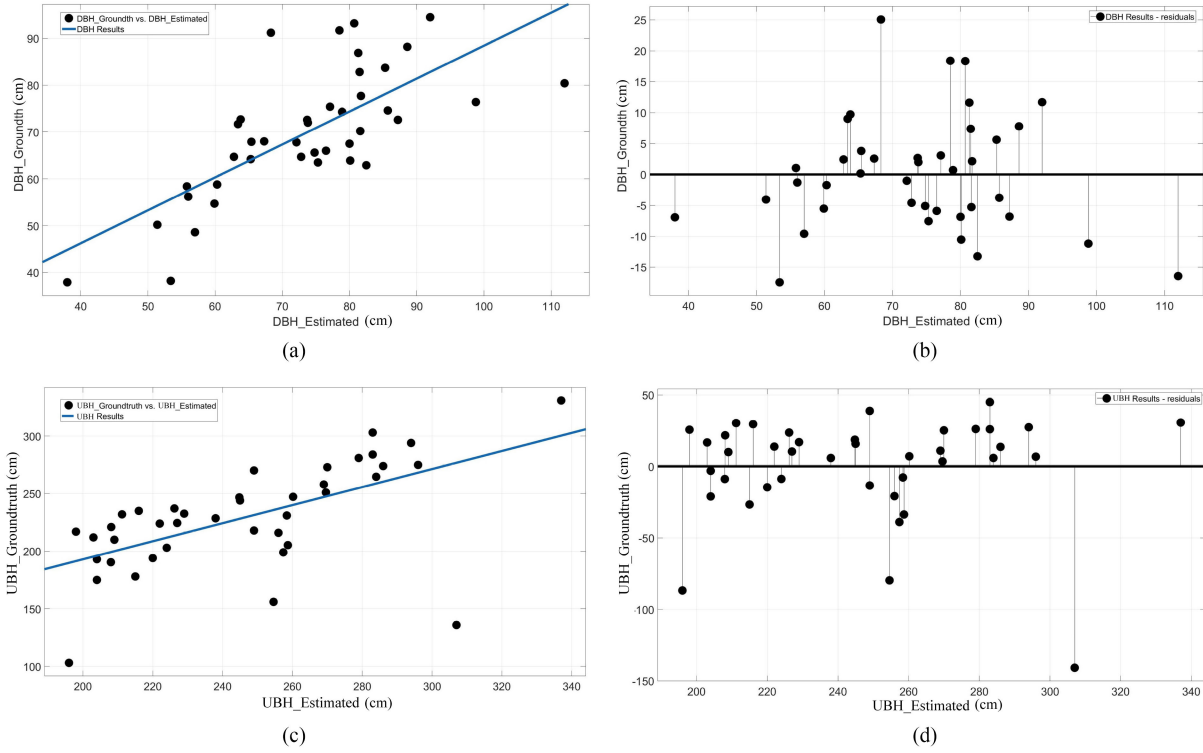
Fig. 8.   Validation of the DBH and UBH estimation. (a) DBH results. (b) Residuals of DBH. (c) UBH results. (d) Residuals of UBH.
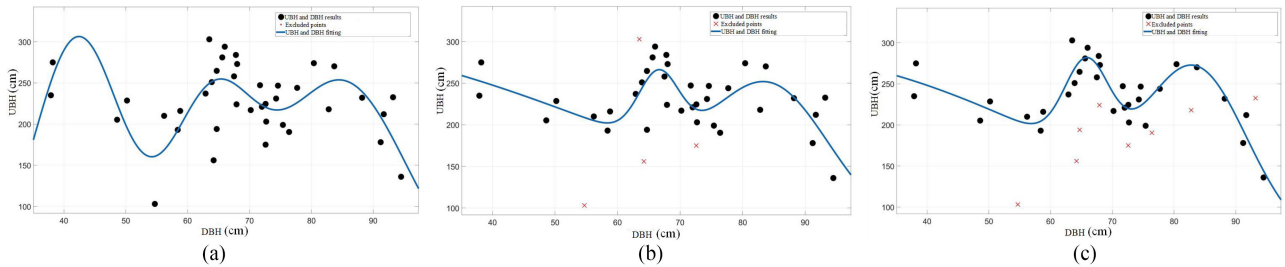

Fig. 9.   Fitting of the relationship between DBH and UBH. (a) Original fitting model. (b) Fitting model by removing 10% outliers. (c) Fitting model by removing 20% outliers.

The following is about the growth level validation. We test three commonly growth models, including the exponential, power, and polynomial model, when the degree of variable x ranges from 1 to 3. In all cases, the R-square is less than 0.10, which means the existing fitting model is not reliable for our street trees, i.e., *Platanus acerifolia* in our experimental scene. Then, we choose the Gaussian function defined as (6) to fit the relationship between DBH and UBH. The fitting figure is shown in Fig. 9(a). The degree is up to 3, the R-square is 0.408, and RMSE is 36.98. Since the chosen degree is 3, we have to discuss the adjusted R-squared, which is a modified version of R-squared that has been adjusted for the number of predictors in the model. It decreases when a predictor improves the model by less than expected by chance. The adjusted R-square is 0.25, which shows the fitting result seems to be promising but still low

$$f(x) = a_1 \cdot e^{-\left(\frac{x-b_1}{c_1}\right)^2} + a_2 \cdot e^{-\left(\frac{x-b_2}{c_2}\right)^2} + a_3 \cdot e^{-\left(\frac{x-b_3}{c_3}\right)^2}. \quad (6)$$

We infer that there are might be errors in data, e.g., system error, random error, or gross error. Therefore, we remove 10% outliers from the Gaussian model and obtain the fitting figure in Fig. 9(b). The achieved R-square is 0.51, adjusted R-square is 0.36, and RMSE is 37.34. If we remove 20% outliers, the achieved R-square is 0.81, adjusted R-square is 0.74, and RMSE is 19.50, as shown in Fig. 9(c). This can be regarded as an effective growth fitting for trees. The obtained coefficients with 95% confidence interval are $a_1 = 107.5$, $b_1 = -0.1734$, $c_1 = 0.3798$, $a_2 = 305.7$, $b_2 = -4.63$, $c_2 = 5.71$, $a_3 = 161.3$, $b_3 = 1.105$, and $c_3 = 0.738$.

Based on fitting results in Fig. 9(c), the R-square is high but the fitting curve is not nondecreasing. This is a huge difference between urban trees and forest trees. In forest trees, the height of a tree with a large DBH is higher than a tree with a small DBH. This means that it is difficult to calculate the *Platanus acerifolia* growth model using methods for the forest trees. A
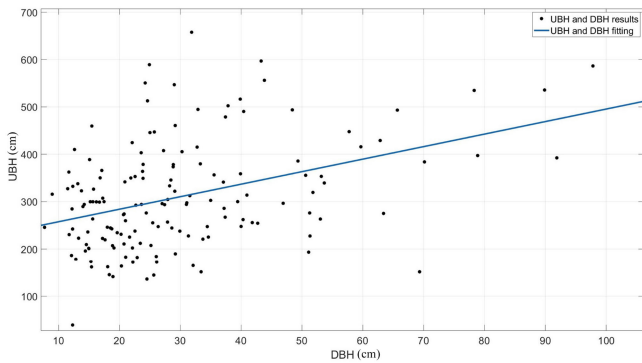
Fig. 10.   Illustration of the DBH and UBH estimation.

large DBH may have a low UBH in street trees. This is because *Platanus acerifolia* is pruned by human beings for the purpose of improving the landscape. 80% of *Platanus acerifolia* with the DBH and UBH of 60–80 cm and 200–300 cm, respectively, for the purpose of a large view and collision-free. Besides, although we know trees are transplanted to Huangpu road in 1929, some of them may die from pests. Therefore, trees that are replanted will turn to be "outliers" to our fitting model. Since street trees are important to green cities, our results can provide a better scheme for the city planning.

In the growth fitting evaluation from VLS, we cannot measure the DBH and UBH by using a tape measure in the experimental plot. The fitting demonstration figure is shown in Fig. 10. We do not have the ground truth, therefore, we can only show the growth fitting based on the estimated DBH and UBH. In the growth level validation, we test the commonly used growth model, including the exponential, power, or polynomial model, when the degree of variable x grows from 1 to 3. In all cases, the R-square is less than 0.2, which means we cannot obtain a valid growth fitting based on the VLS data. This is because the completeness of stems identification from VLS is highly depends on its density. Besides, stems are easy to be occluded by other trees, which will incur an incorrect UBH.

V. CONCLUSION

This study constitutes a practical application of street tree growth fitting using mobile laser scanning data. The result includes the identification of urban trees and the growth fitting of stem structures, which shows that mobile LiDAR data can be used to measure the DBH and the UBH of urban trees. The average RMSE of the achieved DBH and UBH is 9.46 and 36.75 cm, respectively. The growth fitting based on the mapped DBH and UBH is formulated by a Gaussian model effectively. The average R-square and RMSE of the growth fitting are up to 0.81 and 19.5 cm, respectively, which indicates that WLS can be used to urban forest mapping and growth fitting in urban environments.
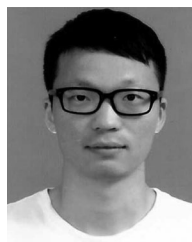
Research shows the increment and growth trend estimation of street trees is quite different from the forest, which can be built by a linear or polynomial model effectively. This is because the

street trees, such as *Platanus acerifolia* in our test, have been pruned by the municipality. It could be expected that improving MLS technologies, increasing density of laser scanning points and data availability will result in improving the accuracy of urban forest growth estimation and biomass calculation. Besides, urban forest management will increasingly rely on 3-D laser scanning data; hence, further considerable research is required to cluster and recognize tree points from 3-D point clouds. Ongoing research is to validate the achieved growth model for street trees in different years and locations. Future research is also necessary to determine whether the experiment can be applied to other street trees in nearby cities.

REFERENCES

[1] G. von Oheimb *et al.*, "Individual-tree radial growth in a subtropical broad-leaved forest: The role of local neighbourhood competition," *Forest Ecology Manage.*, vol. 261, no. 3, pp. 499–507, 2011.

[2] H. Guan, Y. Yu, Z. Ji, J. Li, and Q. Zhang, "Deep learning-based tree classification using mobile LiDAR data," *Remote Sens. Lett.*, vol. 6, no. 10–12, pp. 864–873, 2015.

[3] H. Mak and B. Hu, "Tree species identification and subsequent health determination from mobile LiDAR data," in *Proc. IEEE Int. Geosci. Remote Sens. Symp.*, 2014, pp. 1365–1368.

[4] H. Mak and B. Hu, "Characterization of tree structures from mobile LiDAR data for the identification of ash trees," in *Proc. IEEE Int. Geosci. Remote Sens. Symp.*, 2015, pp. 5371–5374.

[5] T. Yun *et al.*, "Simulation of multi-platform LiDAR for assessing total leaf area in tree crowns," Agricultural Forest Meteorology, vol. 276/277, 2019, Art. no. 107610.

[6] C. Hu, Z. Pan, and P. Li, "A 3D point cloud filtering method for leaves based on manifold distance and normal estimation," *Remote Sens.*, vol. 11, no. 2, 2019, Art. no. 198.

[7] S. Limoges, T. T. H. Pham, and P. Apparicio, "Growing on the street: Multilevel correlates of street tree growth in Montreal," *Urban Forestry Urban Greening*, vol. 31, pp. 15–25, 2018.

[8] I. Seiferling, N. Naik, C. Ratti, and R. Proulx, "Green streets- quantifying and mapping urban trees with street-level imagery and computer vision," *Landscape Urban Planning*, vol. 165, pp. 93–101, 2017.

[9] M. Holopainen *et al.*, "Tree mapping using airborne, terrestrial and mobile laser scanning—A case study in a heterogeneous urban forest," *Urban Forestry Urban Greening*, vol. 12, no. 4, pp. 546–553, 2013.

[10] C. Cabo, S. Del Pozo, P. Rodríguez-Gonzálvez, C. Ordóñez, and D. González-Aguilera, "Comparing terrestrial laser scanning (TLS) and wearable laser scanning (WLS) for individual tree modeling at plot level," *Remote Sens.*, vol. 10, no. 4, 2018, Art. no. 540.

[11] M. Lehtomäki, A. Jaakkola, J. Hyyppä, A. Kukko, and H. Kaartinen, "Detection of vertical pole-like objects in a road environment using vehicle-based laser scanning data," *Remote Sens.*, vol. 2, no. 3, pp. 641–664, 2010.

[12] N. H. Arachchige, "Automatic tree stem detection—A geometric feature based approach for MLS point clouds," *ISPRS Ann. Photogramm. Remote Sens. Spatial Inf. Sci.*, no. 2, pp. 109–114, 2013.

[13] X. Liang, J. Hyyppa, A. Kukko, H. Kaartinen, A. Jaakkola, and X. Yu, "The use of a mobile laser scanning system for mapping large forest plots," *IEEE Geosci. Remote Sens. Lett.*, vol. 11, no. 9, pp. 1504–1508, Sep. 2014.

[14] S. Xia, C. Wang, F. Pan, X. Xi, H. Zeng, and H. Liu, "Detecting stems in dense and homogeneous forest using single-scan TLS," *Forests*, vol. 6, no. 11, pp. 3923–3945, 2015.

[15] L. Zhong, L. Cheng, H. Xu, Y. Wu, Y. Chen, and M. Li, "Segmentation of individual trees from TLS and MLS data," *IEEE J. Sel. Topics Appl. Earth Observ. Remote Sens.*, vol. 10, no. 2, pp. 774–787, Feb. 2017.

[16] S. Pu, M. Rutzinger, G. Vosselman, and S. O. Elberink, "Recognizing basic structures from mobile laser scanning data for road inventory studies," *ISPRS J. Photogramm. Remote Sens.*, vol. 66, no. 6, pp. S28–S39, 2011.

[17] L. Li, D. Li, H. Zhu, and Y. Li, "A dual growing method for the automatic extraction of individual trees from mobile laser scanning data," *ISPRS J. Photogramm. Remote Sens.*, vol. 120, pp. 37–52, 2016.

[18] C. Vega *et al.*, "PTrees: A point-based approach to forest tree extraction from lidar data," *Int. J. Appl. Earth Observ. Geoinf.*, vol. 33, pp. 98–108, 2014.

[19] B. Hu, J. Li, L. Jing, and A. Judah, "Improving the efficiency and accuracy of individual tree crown delineation from high-density LiDAR data," *Int. J. Appl. Earth Observ. Geoinf.*, vol. 26, pp. 145–155, 2014.

[20] Y. Chen *et al.*, "Rapid urban roadside tree inventory using a mobile laser scanning system," *IEEE J. Sel. Topics Appl. Earth Observ. Remote Sens.*, vol. 12, no. 9, pp. 3690–3700, Sep. 2019.

[21] Raumonen *et al.*, "Comprehensive quantitative tree models from terrestrial laser scanner data," *Remote Sens.*, vol. 5, pp. 491–520, Jan. 2013.

[22] J. Hackenberg, C. Morhart, J. Sheppard, H. Spiecker, and M. Disney, "Highly accurate tree models derived from terrestrial laser scan data: A method description," *Forests*, vol. 5, pp. 1069–1105, 2014.

[23] B. Wu *et al.*, "A voxel-based method for automated identification and morphological parameters estimation of individual street trees from mobile laser scanning data," *Remote Sens.*, vol. 5, no. 2, pp. 584–611, 2013.

[24] S. Tao *et al.*, "Segmenting tree crowns from terrestrial and mobile LiDAR data by exploring ecological theories," *ISPRS J. Photogramm. Remote Sens.*, vol. 110, pp. 66–76, 2015.

[25] F. Wu, C. Wen, and J. Li, "Automated extraction of urban trees from mobile LiDAR point clouds," in *Proc. ISPRS Int. Conf. Comp. Vis. Remote Sens.*, Mar. 2016, vol. 9901, pp. 159–164.

[26] Y. Livny, F. Yan, M. Olson, B. Chen, H. Zhang, and J. El-Sana, "Automatic reconstruction of tree skeletal structures from point clouds," *ACM Trans. Graph.*, vol. 29, no. 6, pp. 151–158, 2010.

[27] X. Zhang, H. Li, M. Dai, W. Ma, and L. Quan, "Data-driven synthetic modeling of trees," *IEEE Trans. Vis. Comput. Graph.*, vol. 20, no. 9, pp. 1214–1226, Sep. 2014.

[28] Z. Wang *et al.*, "A structure-aware global optimization method for reconstructing 3-D tree models from terrestrial laser scanning data," *IEEE Trans. Geosci. Remote Sens.*, vol. 52, no. 9, pp. 5653–5669, Sep. 2014.

[29] Z. Wang *et al.*, "A local structure and direction-aware optimization approach for three-dimensional tree modeling," *IEEE Trans. Geosci. Remote Sens.*, vol. 54, no. 8, pp. 4749–4757, Aug. 2016.

[30] S. Xu, S. Xu, N. Ye, and F. Zhu, "Automatic extraction of street trees' non-photosynthetic components from MLS data," *Int. J. Appl. Earth Observ. Geoinf.*, vol. 69, pp. 64–77, 2018.

[31] X. Yang, H. Yang, F. Zhang, X. Fan, Q. Ye, and Z. Feng, "A random-weighted plane-Gaussian artificial neural network," *Neural Comput. Appl.*, vol. 31, no. 12, pp. 8681–8692, 2019.

[32] C. Feng, Y. Taguchi, and V. R. Kamat, "Fast plane extraction in organized point clouds using agglomerative hierarchical clustering," in *Proc. IEEE Int. Conf. Robot. Autom.*, 2014, pp. 6218–6225.

[33] R. Schnabel, R. Wahl, and R. Klein, "Efficient RANSAC for point-cloud shape detection," *Comput. Graph Forum*, vol. 26, no. 2, pp. 214–226, 2007.

[34] B. Vallet, M. Brédif, A. Serna, B. Marcotegui, and N. Paparoditis, "TerraMobilita/iQmulus urban point cloud analysis benchmark," *Comput. Graph.*, vol. 49, pp. 126–133, 2015.

[35] H. Guan, Y. Yu, J. Li, and P. Liu, "Pole-like road object detection in mobile LiDAR data via supervoxel and bag-of-contextual-visual-words representation," *IEEE Geosci. Remote Sens. Lett.*, vol. 13, no. 4, pp. 520–524, Apr. 2016.

[36] F. Wu *et al.*, "Rapid localization and extraction of street light poles in mobile LiDAR point clouds: A supervoxel-based approach," *IEEE Trans. Intell. Transp. Syst.*, vol. 18, no. 2, pp. 292–305, Feb. 2017.

Sheng Xu received the B.Eng. degree in computer science and technology from Nanjing Forestry University, Nanjing, China, in 2010, and the Ph.D. degree in digital image systems from the University of Calgary, Calgary, AB, Canada, in 2018.

In 2018, he joined the College of Information Science and Technology, Nanjing Forestry University, where he is currently an Associate Professor. His current research interests include mobile mapping, vegetation mapping, and computer vision.

Xinyu Sun received the B.S. degree in geographic information science, in 2018 from Nanjing Forestry University, Nanjing, China, where she is currently working toward the Doctorate degree with the College of Forestry.

Her research interests include eco-environment remote sensing and vegetation mapping.

Jiayan Yun received the Ph.D. degree in landscape architecture from the Seoul National University, Seoul, South Korea, in 2018.

She joined the College of Landscape Architecture, Nanjing Forestry University, Nanjing, China, as an Assistant Professor, in 2018. Her current research interests include cultural landscape, digital conservation of cultural landscape heritage, and history and theory of landscape architecture.

Hao Wang received the B.Eng. degree from Tongji University, Shanghai, China, in 1983, and the Ph.D. degree from Nanjing Forestry University, Nanjing, China, in 2001.

He joined the College of Landscape Architecture, Nanjing Forestry University, in 1983, where he is currently a Professor. His research interests include landscape architecture design, urban planning, and green space system analysis.

Dr. Wang is a member of the Editorial Committee of Chinese Landscape Architecture.